photonics

MDPI

Article

Dynamics Simulation of Self-Mode-Locking in a Semiconductor Disk Laser Using Delay Differential Equations

Tao Wang [1], Renjiang Zhu [1], Cunzhu Tong [2], Yunjie Liu [3] and Peng Zhang [3,*]

[1] College of Physics and Electronic Engineering, Chongqing Normal University, Chongqing 401331, China
[2] Changchun Institute of Optics, Fine Mechanics and Physics, Chinese Academy of Sciences, Changchun 130033, China
[3] National Center for Applied Mathematics in Chongqing, Chongqing Normal University, Chongqing 401331, China
* Correspondence: zhangpeng2010@cqnu.edu.cn

Abstract: Self-mode-locked semiconductor disk lasers possess compact resonant cavity and stable construction. These devices have a wide application prospect because of their picosecond to sub-picosecond pulse width, excellent beam quality and tailorable emission wavelength. In this paper, dynamics simulations of self-mode-locking in a semiconductor disk laser are performed by using delay differential equations for the first time. The corresponding conditions of different modality of mode-locking, including Q-switched mode-locking, continuous-wave mode-locking and harmonic mode-locking are calculated, and their dynamics evolution processes are presented. We also analyze the characteristics of the three different mode-locking modalities and summarize their overall dynamics evolution tendency. This kind of numerical simulation and analysis provides an understanding of the dynamics process of self-mode-locking, and may be referenced for related experiments.

Keywords: semiconductor disk laser; self-mode-locking; dynamics simulation; delay differential equations

Citation: Wang, T.; Zhu, R.; Tong, C.; Liu, Y.; Zhang, P. Dynamics Simulation of Self-Mode-Locking in a Semiconductor Disk Laser Using Delay Differential Equations. *Photonics* **2022**, *9*, 859. https://doi.org/10.3390/photonics9110859

Received: 17 October 2022
Accepted: 10 November 2022
Published: 13 November 2022

1. Introduction

Semiconductor disk lasers (SDLs) are perfectly suitable for the generation of ultrashort pulses with pulse duration from picosecond to sub-picosecond and a pulse repetition rate at a gigahertz magnitude because of their intrinsic time characteristics of carriers [1–3]. Mode-locked SDLs combine key features such as good beam quality, moderate output power, ultrashort pulse duration, steady pulse amplitude and tailorable emission wavelength, while maintaining their construction simplicity and mechanism stability [4,5]. They are of great interest for different applications, including biophotonics [6], spectroscopy [7] and laser cooling and trapping [8].

Since the first passively mode-locked SDL was reported [9], performances of such devices have been greatly improved. The maximum average output power has been increased to 6.4 W [10], the minimum pulse width has been decreased to 60 fs [11], and the repetition rate directly arisen from an oscillator has been pushed to 101.2 GHz [12]. Many groups have also done excellent research on the mechanism of passively mode-locking (ML) in a SDL, e.g., the effect of dispersion [13] and the nonequilibrium carrier dynamics [14]. Those passively mode-locked solid-state and fiber lasers can produce some wavelengths for specific utilizations, use saturate absorbers made of various new materials, and obtain high single-pulse energy by reducing the repetition rate [15–18]. In contrast, mode-locked and Q-switched semiconductor disk lasers have more flexible and designable emission wavelengths, higher average output power and pulse repetition rate.

In addition to the passive ML based on a semiconductor saturable absorption mirror (SESAM), researchers have found another method for ML in SDLs: self-mode-locking (SML) [19,20]. Some experiments of SML require inserting a slit or another Kerr medium

into a laser resonator [21,22], while other reports of SML do not require placing any additional elements into the cavity [23–25].

Currently, it is widely accepted that SML in an SDL originates from the Kerr effect in a semiconductor gain medium [26,27]. The Kerr effect means that the refractive index of medium changes nonlinearly with the electric intensity, but linearly with the light intensity of an incident laser, i.e., $n = n_0 + n_2 I$. Where n_0 is the refractive index without light, I represents the light intensity, and n_2 is the nonlinear refractive index. In solid-state lasers, the refractive index of a crystal depends on the real part of complex dielectric function. Because the response time of polarization in crystal can be almost ignored, the Kerr-lens (caused by the change of refractive index) and the hard (or soft) aperture in the laser cavity constitute a "fast" saturable absorber, which can start the SML and produce a pulse width of femtosecond magnitude [28].

For semiconductor lasers, the situation is slightly different. The nonlinear refractive index of semiconductor gain medium is caused by the change of carrier concentration. As the inter- and intra-band relaxation time of carriers are in the order of nanoseconds and picoseconds [29], the recovery time of the saturable absorber formed by the Kerr-lens and an aperture in a semiconductor laser is not as fast as that in a solid-state laser. In the numerical simulations in this paper, we will consider the Kerr-lens along with an aperture in self-mode-locked SDL as a "slow" saturable absorber, i.e., a saturable absorber with a recovery time similar to a SESAM.

There have been many reports on the numerical analysis of the physical mechanism and dynamic process of SESAM mode-locked SDLs. A fully microscopic model was used to investigate the transverse mode instabilities and the ultrafast nonequilibrium carrier dynamics of electron-hole excitations in a semiconductor quantum-well gain and absorber [14,30,31]. The rate equation method was employed to disclose the soliton-like pulse-shaping mechanism and harmonically ML [13,32]. An extended master equation approach based on partial differential equations was introduced to describe the complex pulse train and the influence of group velocity dispersion on the stability boundary [33].

The delay differential equations (DDEs), which have been successfully used to describe various dynamics systems, were also utilized to investigate a passively mode-locked SDL. DDEs have been employed to verify the fundamental and soliton bound states in a low repetition rate mode-locked SDL [34], to depict the pulse cluster dynamics [35], and to explain the dispersive instability and ML behavior in an SDL with different cavity configurations [36,37].

As a new method for ML in SDLs, SML has not yet been numerically simulated. In this paper, the DDEs, a powerful mathematical tool suitable for describing dynamics systems, is used to conduct a comprehensive simulation and analysis of the SML in SDLs. This work mainly includes the calculation of the dynamics process of three different ML regions: the Q-switched ML, the continuous-wave (CW) ML and the harmonic ML. A related analysis of condition and the corresponding performance of the above three ML regions are also presented. This kind of numerical simulation and analysis provides some understanding as to the dynamics process of SML and may be referenced for related experiments.

2. Delay Differential Equations for Passively ML

The dynamics of ML can be well explained by Haus master equations [38]. This analytical approach is widely used because of its insight into the underlying mechanism of ML. However, the dynamics of some mode-locked lasers (e.g., fiber lasers and semiconductor lasers) can no longer be described satisfactorily by the master equation because it is based on small changes of gain and losses in a laser pulse shape within one round-trip. In comparison, DDEs, which have been successfully used to describe various dynamics systems, can effectively reproduce the dynamics while circumventing the approximation of small gain and loss. Here we use the DDEs model proposed by A. G. Vladimirov et al. for passively mode-locked semiconductor lasers [39,40]. This model avoids the approximation of small

gain and loss per cavity round-trip, and is closer to the actual condition of semiconductor laser devices.

The DDEs can be expressed as:

$$\frac{1}{\gamma}\frac{\partial A}{\partial t} = \sqrt{\kappa}\exp\left\{\frac{1}{2}[(1-i\alpha_g)g(t-\tau)-(1-i\alpha_q)q(t-\tau)]\right\}A(t-\tau)-A(t) \quad (1)$$

$$\frac{\partial g}{\partial t} = \gamma_g(g_0-g(t))-\exp(-q)[\exp(g)-1]|A(t)|^2 \quad (2)$$

$$\frac{\partial q}{\partial t} = \gamma_q(q_0-q(t))-s[1-\exp(-q)]|A(t)|^2 \quad (3)$$

where A is the electric field amplitude of the laser. γ is the bandwidth of the spectral filter. κ describes the total nonresonant linear intensity loss per cavity round-trip. α_g and α_q are linewidth enhancement factors for the gain medium and saturable absorber, respectively. g and q indicate time dependent saturable gain and absorption. g_0 and q_0 denote the initial value of g and q. γ_g and γ_q are relaxation rate in the gain and absorber, and s is the ratio of saturation energy of the gain and absorber. It should be noted that the delay parameter τ is equal to the cavity round-trip time, and in this work, all times in the above equations are normalized by the cavity round-trip time.

3. Simulation Results and Discussions

3.1. Determination of Parameters

In the subsequent numerical simulations, we try to make parameters consistent with reported or commonly used experimental data as much as possible, so that the numerical simulation results have broader suitability. We choose a linear resonator composed of a distributed Bragg reflector (DBR) at the bottom of the gain chip and an external flat-concave end mirror with a 150 mm curvature radius. The high-reflection coated end mirror has a reflectivity of R_1 = 99.9% at the laser wavelength, and the reflectivity of the bottom DBR for the laser wavelength is about R_2 = 99%. In the DDEs (1)–(3), κ is defined as the fraction of power remaining in the cavity after each round-trip. So, we have $\kappa = \sqrt{R_1 R_2} = 0.9945$.

According to the existing research results, the linewidth enhancement factors α_g and α_q will slightly change the mode-locked region and pulse width [39–41], which is also obvious in theory. There is no real saturable absorber for a self-mode-locked semiconductor disk laser (SDL) discussed in this paper. The "equivalent saturable absorber" utilized in a SDL to start mode-locking is composed of the Kerr lens in the gain medium and the soft aperture provided by the pump spot. In this sense, the gain is also the saturable absorber. Therefore, we approximately assume that α_g is equal to α_q, thus ignoring their influence on the calculation results, i.e., both α_g and α_q are chosen to be zero in the simulation [39–41]. For a generally used SDL with emission wavelength at 1 μm waveband, the active region consists of InGaAs multiple quantum wells, which is similar to that in reference [35], so the value of gain bandwidth can be selected as 10 nm and the corresponding bandwidth of the spectral filter is γ = 200.

Since the radius of curvature of the output coupler is provided to be 150 mm, for a frequently used value of 200 μm diameter of the pump spot, the cavity length meeting the match-condition of the laser and pump spot on the gain chip is about 145 mm. This results in an approximate cavity round-trip time of τ_r~1 ns. Considering that the typical value of the gain recovery time can be chosen as 10 ns, and it should be normalized by τ_r as mentioned before, the relaxation rate of gain medium will be γ_g = 0.1. As for the value of g_0, it is determined by referring to the literature [39–41].

The parameter selection of a saturable absorber is a little more complicated, because there is no real saturable absorber in a self-mode-locked SDL, but an equal saturable absorber composed of an equivalent Kerr-lens and a soft aperture. With a provided pump power (i.e., a given focal length of the Kerr-lens), the primary mean to change the modulation depth of a saturable absorber is to change the size of the soft aperture. That is, to change the size

of overlapping area between the pump and laser spot. To obtain the above modulation, we suppose a pump power of 10 W and a pulse peak power of 50 kW, which correspond to 250 W intracavity circulating power and 250 mW average output power when the transmittance of output coupler is 0.1%, the pulse width is 5 ps and the pulse repetition rate is 1 GHz) [19,20,26,42]. First, the nonlinear refractive index n_2 of gain medium under different pump spot sizes is calculated according to the data provided by reference [43]. The results are shown by the green dotted line in Figure 1 (the coordinate axis of n_2 is not shown). Then, based on the focal length formula of the Kerr-lens $f = \omega^2/(4\pi n_2 I_p L)$ (where ω is the radium of light spot, I_p is the peak light intensity and L is the length of Kerr medium), the focal length of the equivalent Kerr-lens is computed and plotted as the blue solid line in Figure 1. Finally, by using the light field transmission formula and the split-step Fourier method, the amplitude of the light field is calculated when it completes a round-trip in the cavity, and the difference of round-trip loss experienced by the laser beam with (pulse operation) and without (free running) the Kerr-lens is carried out, as shown by the red solid line in Figure 1.

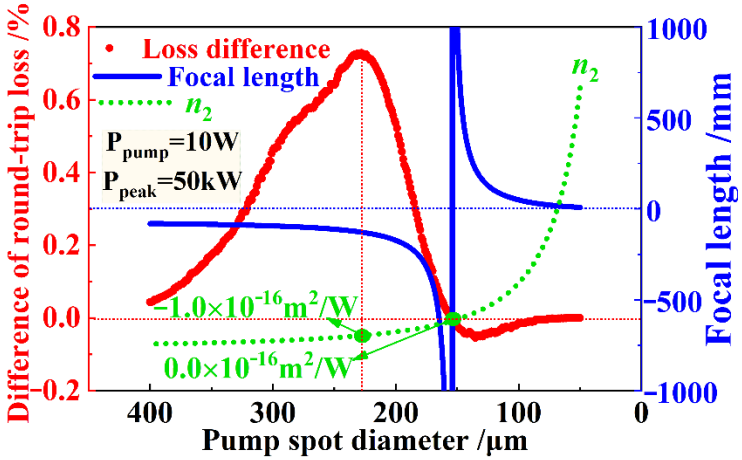

Figure 1. The calculated nonlinear refractive index n_2 of gain medium, focal length f of Kerr-lens, and the difference of round-trip loss with and without Kerr-lens under various pump spot sizes. The pump power and the peak power of noise pulse are supposed to be 10 W and 50 kW, respectively. The nonlinear reflective index n_2 is obtained from reference [42].

It can be seen from Figure 1 that the nonlinear reflective index n_2 increases monotonously with decreasing pump spot size. Its value changes from negative to positive, and it is zero when the pump spot diameter is about 150 μm. Accordingly, when the value of n_2 is negative, the absolute value of focal length increases with decreasing pump spot size, but the absolute value of focal length drops with falling pump spot size when n_2 is positive. Obviously, the focal length of the Kerr-lens is infinite when n_2 equals zero.

The most important parameter, the difference of round-trip loss with and without the Kerr-lens, first goes up with decreasing pump spot, reaches the maximum of 0.7% when the pump spot is about 230 μm, and then comes down with decreasing pump spot. Theoretically, the greater the loss difference, the easier it is to start ML. Therefore, under conditions given in Figure 1, the optimal value of the pump spot should be about 230 μm. The existence of maximum value of loss difference is understandable. On the one hand, a smaller pump spot (i.e., a smaller soft aperture) is favorable for a focused beam because it can introduce more loss to an ordinary beam and provide larger loss difference between the case with and without the Kerr-lens. On the other hand, a smaller pump spot also means a higher pump power density, which will result in a smaller n_2 and thus a longer focal length of the Kerr-lens (because when the pump power density is increased, n_2 will change from negative to positive, and its absolute value will first decrease and then increase [42]). This will raise the loss of focused beam, thus weakening the increase trend of loss difference. So, as can be seen from Figure 1 that the difference of round-trip loss with and without

Kerr-lens has a peak value at 230 μm pump spot, whose pump density corresponds to a n_2 about -1.0×10^{-16} m^2/W. Further reducing of the pump spot will lead to a gradual decrease of loss difference. When the pump spot is reduced to about 150 μm, n_2 is zero, the focal length of the Kerr-lens is infinite, and the corresponding loss difference is reduced to zero.

The calculated round-trip loss difference of the beam with and without the Kerr-lens in Figure 1 is introduced by the equivalent saturable absorber, and can be regarded as the modulation depth of an actual SESAM. In this sense, parameter q_0 in DDEs for a self-mode-locked SDL can be determined by using the above method.

Obviously, SML in a SDL depends on the equivalent saturable absorber, which relies on the Kerr-lens, i.e., the nonlinear refractive index n_2. In view of the fact that the nonlinear refractive index n_2 in the semiconductor gain medium is essentially caused by the carrier density, and its recovery time is totally the same as in a SESAM, whose typical value of recovery time is about 10 ps, therefore the recovery time of the equivalent saturable absorber is chosen to be 10 ps. After being normalized by the cavity round-trip time tr of 1 ns, the value of relaxation rate of absorber is $\gamma_q = 100$.

Parameter s is defined as $s = E_{sat,g}/E_{sat,q}$, and the saturation energy of gain is selected to be $E_{sat,g} = 50$ nJ (corresponding to a spot radius in the order of 100 μm) [13]. Since the equivalent saturable absorber consists of a Kerr-lens and a soft aperture, the parameter $E_{sat,q}$ in this paper is estimated using the critical power of Kerr effect, which can be expressed as $P_{cr} = \pi(0.61)^2\lambda^2/(8n_0n_2)$ [43,44]. For $\lambda = 1000$ nm, GaAs material system $n_0 = 3.5$, $n_2 = -1 \times 10^{-16}$ m^2/W [42,45], and pulse width of 5 ps, the above P_{cr} corresponds to a saturation energy of about 2 nJ, so the estimated value of the saturation parameter is $s = 25$.

All parameters used in simulations below are summarized and listed in Table 1. Linewidth enhancement factors for gain medium and the saturable absorber are not included as mentioned before. Parameter g_0 can be changed with various pump intensity. q_0 can also be changed with different pump intensity, because the pump intensity will change the nonlinear refractive index of gain medium, thus changing the focal length of the Kerr-lens and having an influence on the value of q_0. In addition, q_0 will be obviously affected by the radium of soft aperture. Except g_0 and q_0, other parameters remain a fixed value in numerical simulation.

Table 1. The parameters used in the simulations.

γ	κ	γ_g	γ_q	g_0	q_0	s	α_g	α_q
200	0.9945	0.1	100	0.5–6.5	0.02–4.5	25	0	0

3.2. Q-Switched ML

In a mode-locked SDL, although the carrier relaxation time of nanosecond order can effectively suppress the Q-switching tendency, if the gain of laser is not sufficient, or, the modulation depth of saturable absorber is relatively large, it will still cause undersaturation of the absorber and result in Q-switching.

Particularly, in a self-mode-locked SDL which is initiated by the combined action of a Kerr-lens and a soft aperture, not only the change of pump intensity will lead to the change of focal length of Kerr-lens, the size of soft aperture is also very sensitive to adjustment of the laser cavity. Both may stimulate the Q-switching tendency.

We numerically solve Equations (1)–(3) using the famous Runge-Kutta method, and the simulated Q-switched ML with $q_0 = 2.0$ and various g_0 are plotted in Figure 2. The horizontal axis is time (normalized by the cavity round-trip time t_r), and the longitudinal axis is amplitude of light field (arbitrary unit). Figure 2a–e show the Q-switching envelope of mode-locked pulses in a longer time region, and (f–j) are their corresponding pulse train in a shorter time scale.

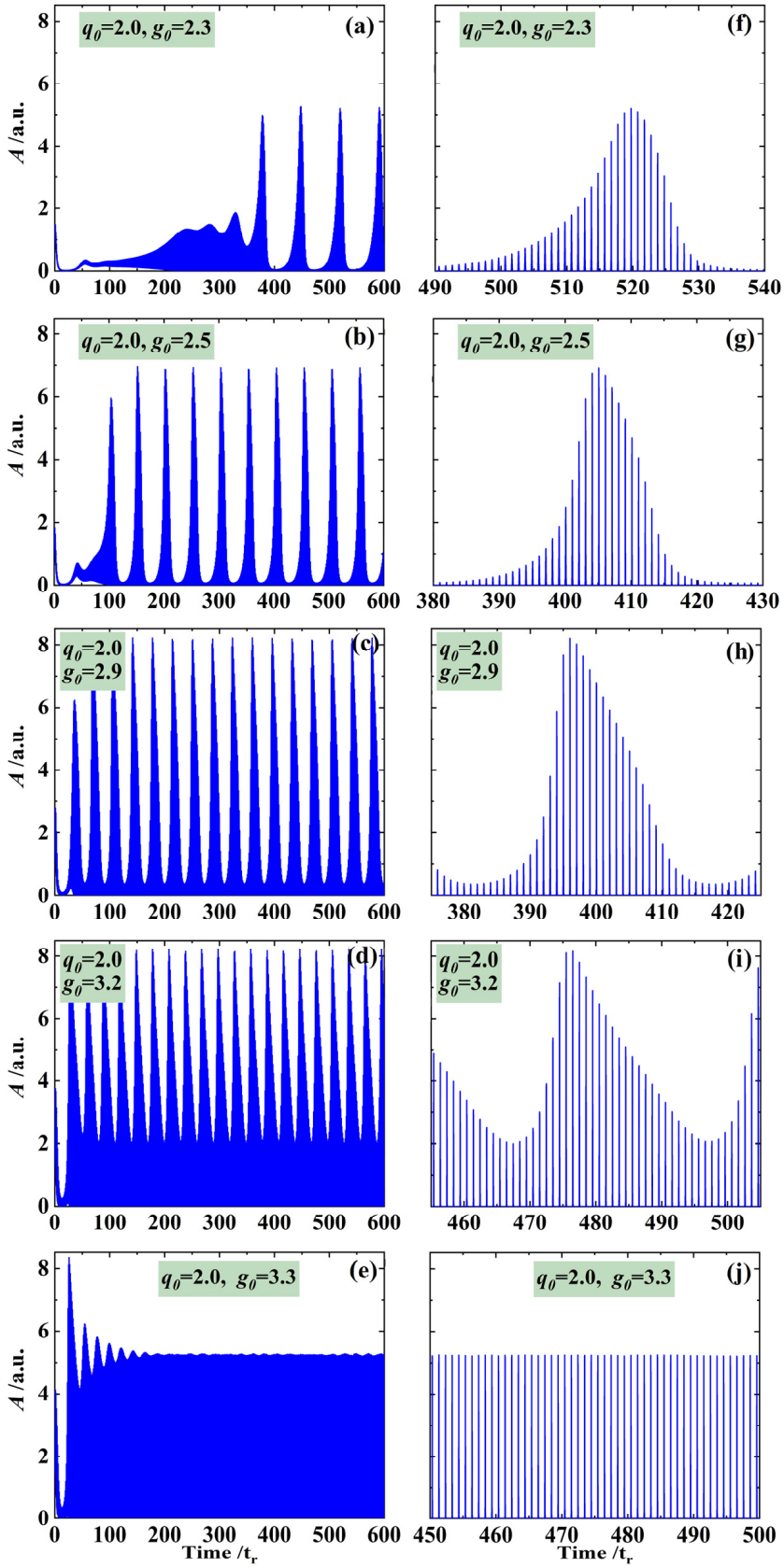

Figure 2. Simulated Q-switched ML with q_0 = 2.0 and various g_0. (**a**) g_0 = 2.3, (**b**) g_0 = 2.5, (**c**) g_0 = 2.9, (**d**) g_0 = 3.2, (**e**) g_0 = 3.3. Figure (**f**–**j**) on the right display the corresponding pulse trains of (**a**–**e**) in a shorter time range.

In Figure 2, with gradually increased gain parameter g_0, the transition from Q-switched ML to CW ML is very clear. The period T_Q (in t_r) of amplitude envelope and the relative modulation depth (in percentage, defined as the difference of maximum and minimum value of amplitude envelope divided by the maximum value) with different g_0 are shown in Figure 3. Obviously, both the period and the modulation depth decrease with increased g_0. It can be expected from Figure 3 that when g_0 reaches a critical point, T_Q and modulation depth will both fall to zero; that is, the ML will transition from Q-switched ML to CW ML. This point is clearly verified in Figure 2e,j, in which g_0 = 3.3, the modulation depth of Q-switch envelope decreases sharply to a negligible value after about 200 round-trips, and the amplitude of pulse train does not change any longer.

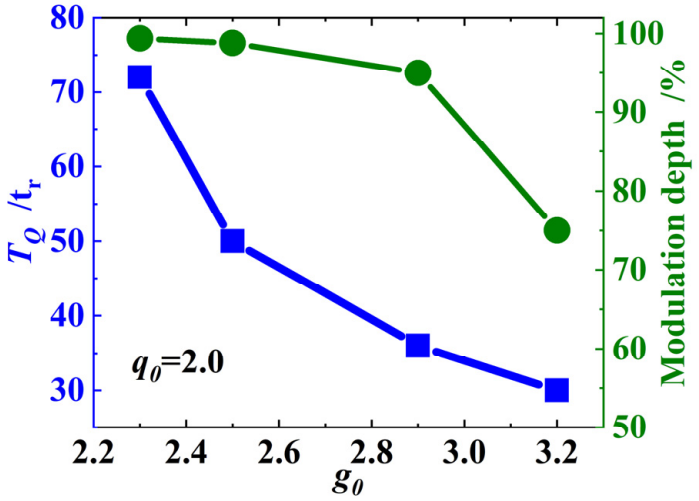

Figure 3. The period T_Q (in t_r) of amplitude envelope and the relative modulation depth (in percentage) in Q-switched ML with q_0 = 2.0 and various g_0.

Both inadequate pump intensity and excessive absorption will result in undersaturation of the absorber. They are mainly responsible for the appearance of Q-switch in ML. Figure 4a shows the undersaturated absorption, the step-by-step saturated gain, and the amplitude-modulated pulse train in Q-switched ML. Within an envelope in Figure 4a, the absorber cannot be fully saturated in a single absorption because of the insufficient pulse energy in the cavity due to the insufficient gain. The gain is not fully saturated too, but changes step by step. Therefore, the net gain windows formed by the combined action of absorption and gain saturation also change gradually. Thus, the amplitudes of established pulses are modulated by an envelope, i.e., Q-switch. Figure 4b shows the formation of two pulses in corresponding net gain windows in detail. It should be noted that their amplitudes are not equal.

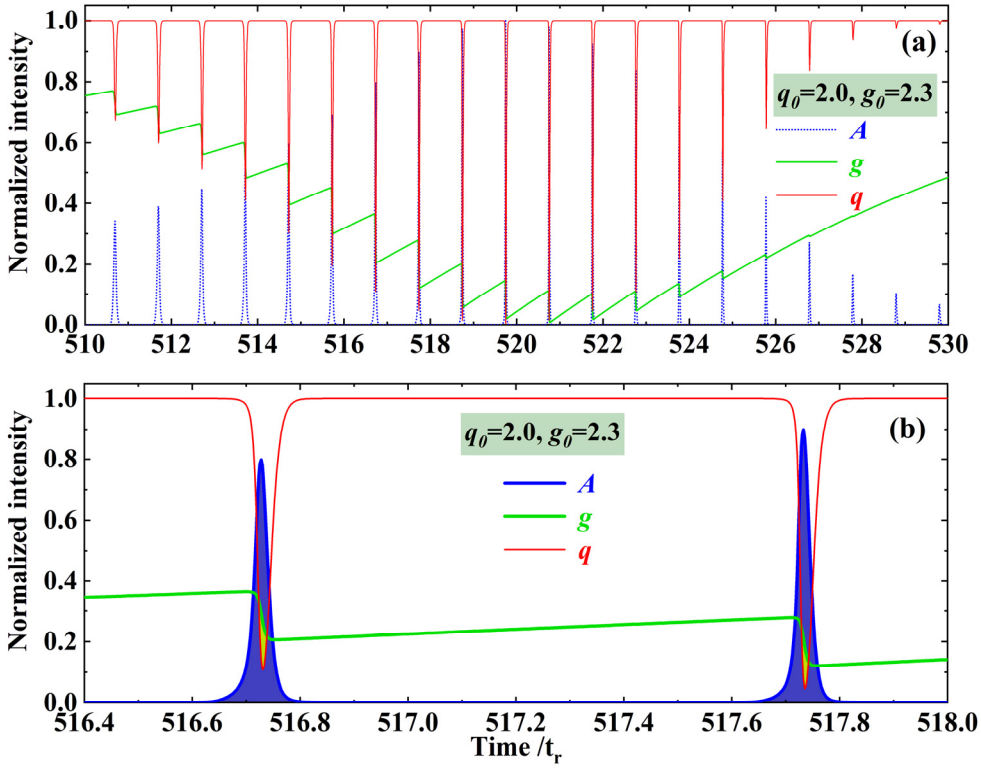

Figure 4. (**a**) Undersaturated absorption, step by step saturated gain, and corresponding amplitude-modulated pulse train in Q-switched ML. (**b**) Formation of two pulses in corresponding net gain windows. It should be noted that their amplitudes are not equal.

3.3. CW ML

The role of the saturable absorber is to promote a mode from noise and stabilize the pulses once they are generated. It has been concluded from previous simulations that both insufficient gain and excessive absorption will cause Q-switching in SML. If CW ML is to be started, two conditions must be met: adequate intracavity circulating power and an aperture with appropriate size. The former can ensure that there is desired noise with enough peak power to generate the necessary Kerr effect, and the latter can provide a certain difference between the round-trip losses of ML and continuous operation, so as to initiate and stabilize ML.

Figure 5a–e show the evolution of calculated CW mode-locked pulses under different g_0 when q_0 = 0.5. Figures on the right side describe performance of the pulses in a smaller time range. As can be seen from Figure 5, if g_0 is relatively small (figure (a)) or large (figure (e)), the time required for building a stable pulse is relatively longer. In all CW ML processes, the pulse amplitude gradually increases while the pulse width also increases with increased g_0, as shown in Figure 6. Although the simulated pulse width cannot be strictly equal to that produced from the experiment (in fact, most reported pulse widths in SML are far small than the calculated pulse width here), the trend that pulse width increases with increased g_0 in numerical simulation still has certain reference significance for experimental design.

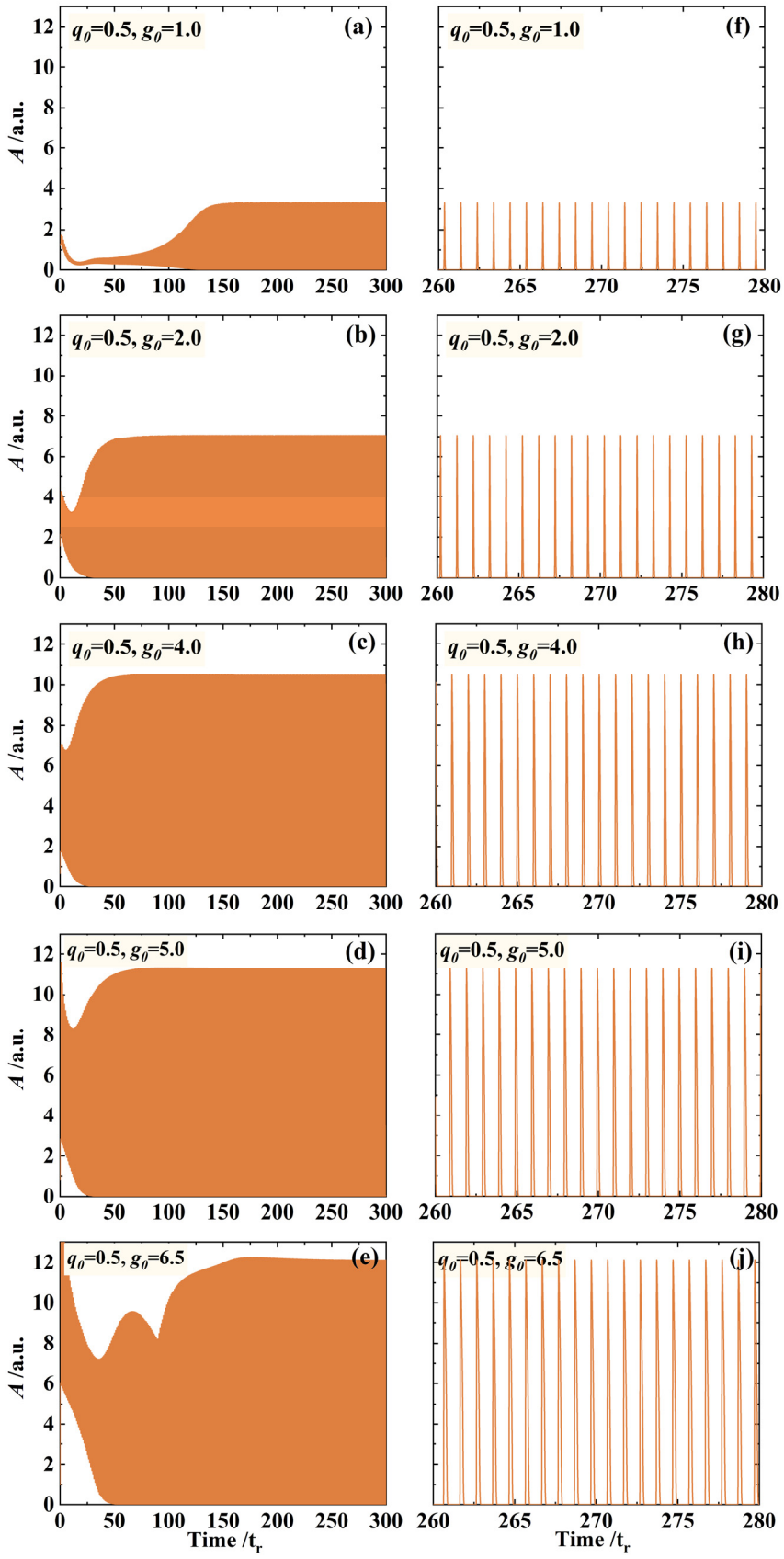

Figure 5. Evolution of calculated CW mode-locked pulses under different g_0 when q_0 = 0.5. (**a**) g_0 = 1.0, (**b**) g_0 = 2.0, (**c**) g_0 = 4.0, (**d**) g_0 = 5.0, (**e**) g_0 = 6.5. Figure (**f**–**j**) on the right side describe performance of the pulses of (**a**–**e**) in a smaller time range.

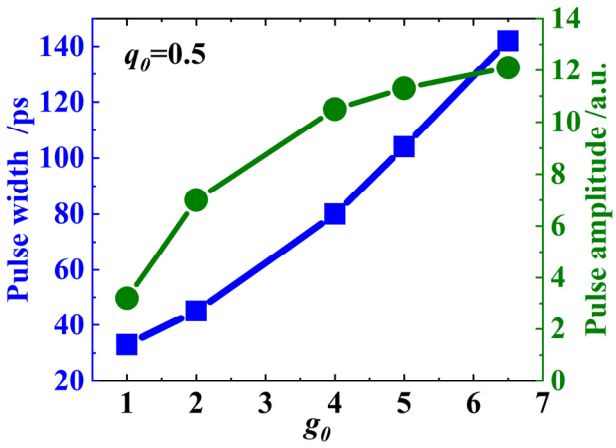

Figure 6. Simulated pulse width and pulse amplitude with q_0 = 0.5 and varied g_0 from 1.0 to 6.5.

We plot the establishment process of pulse in the corresponding net gain window in Figure 7a. Compared with Figure 4b, because the absorber and gain can be fully saturated here, the net gain window is deeper, and the pulse amplitude is higher and uniform. Figure 7b shows that when the gain is too large or the pump is too intense, building-up of a steady pulse train needs to undergo more oscillation. In the second harmonic region marked in Figure 7b, pulses have already been split and the second harmonics have appeared. However, the gain is not sufficient to maintain the second harmonics, which disappears after about 100 intracavity round-trips. Finally, the pulses tend to stable fundamental ML. It can be expected that a robust harmonic ML can be achieved by increasing the pump intensity, as described later.

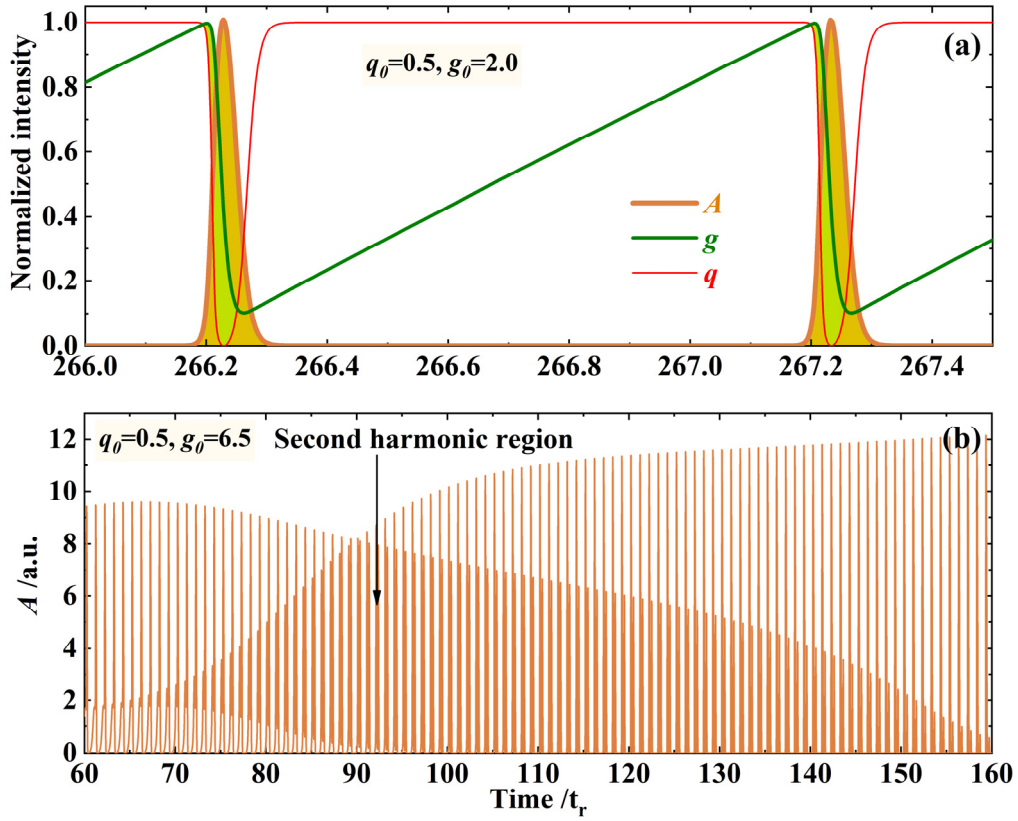

Figure 7. Establishment process of pulse in the corresponding net gain window (**a**). With q_0 = 0.5 and a relatively large g_0 = 6.5, second harmonics begin to emerge and then disappears (**b**).

3.4. Harmonic ML

As mentioned above, when the gain is enlarged to a certain extent, pulse will be split and stabilized, and the CW ML in SML will change to harmonic ML. Figure 8a–d show the second harmonic ML obtained by different permutation of g_0 and q_0, where the value of g_0 is about 20 times that of q_0. Figure 8e–h on the right side are their corresponding pulses within ten round-trips. It can be concluded from Figure 8 that the pulse width will decrease with raising g_0 and q_0, and permutations of larger or smaller g_0 and q_0 all will need more intracavity cycles for harmonic ML to reach a stable state.

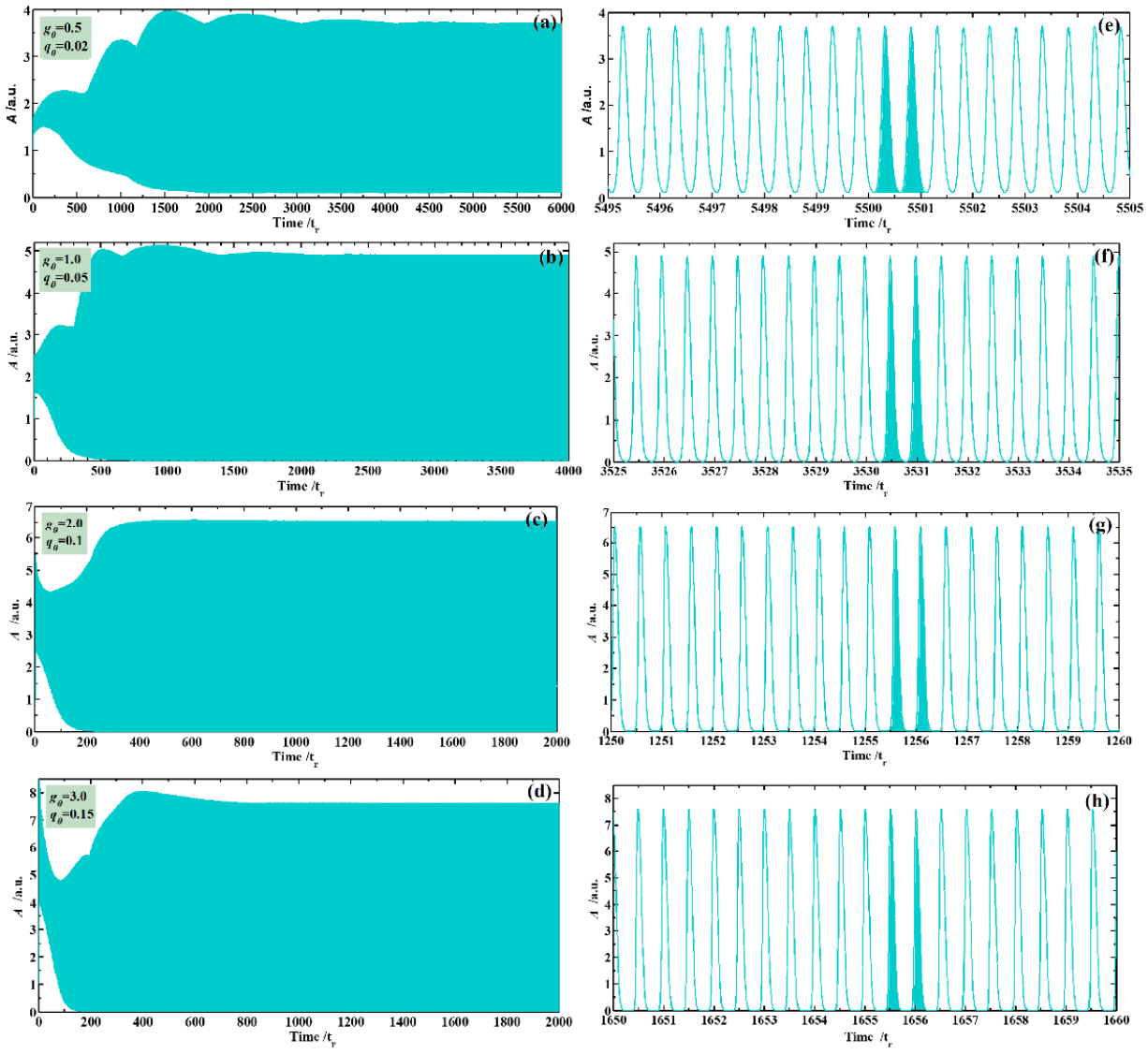

Figure 8. Second harmonic ML obtained by different permutation of g_0 and q_0. (**a**) g_0 = 0.5, q_0 = 0.02, (**b**) g_0 = 1.0, q_0 = 0.05, (**c**) g_0 = 2.0, q_0 = 0.1, (**d**) g_0 = 3.0, q_0 = 0.15. (**e**–**h**) on the right side are their corresponding pulses within ten round-trips.

Figure 9a,b indicate the emergence and gradual enhancement of the second harmonic in a shorter and longer time range when g_0 = 2 and q_0 = 0.1. The second harmonic becomes steady after about 350 intracavity round-trips and maintains the same amplitude as the fundamental wave. Figure 9c shows the establishment of two intracavity circulating pulses in the corresponding net gain windows formed by the successively saturated absorption and gain.

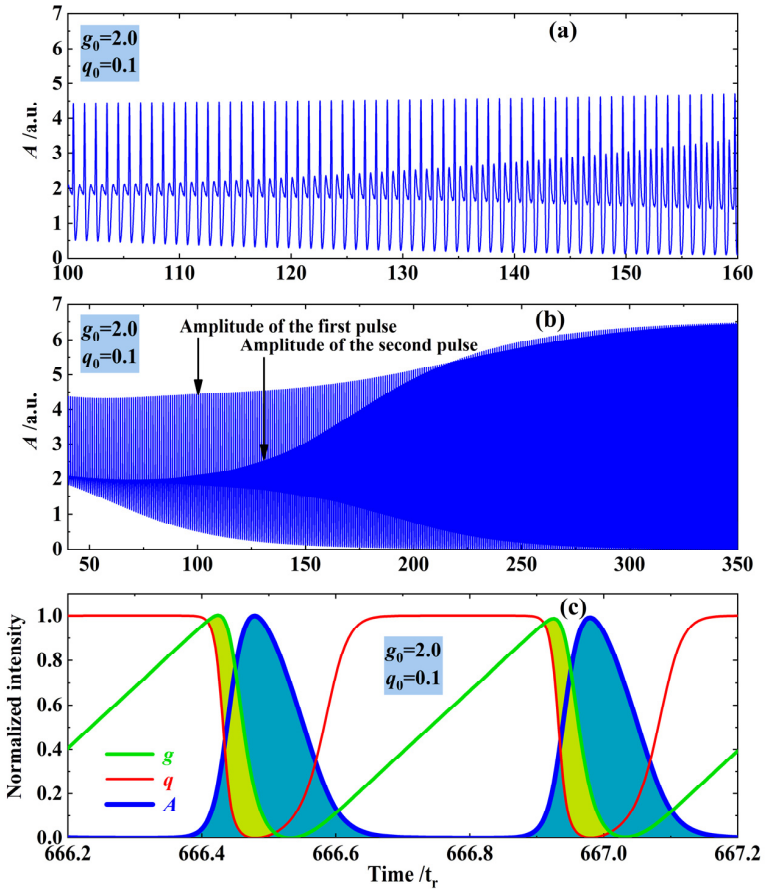

Figure 9. Emergence (**a**) and enhancement (**b**) of the second harmonic when g_0 = 2 and q_0 = 0.1. (**c**) establishment of two intracavity circulating pulses.

Increasing the values of g_0 and q_0 and keeping the ratio of g_0 to q_0 roughly the same when the second harmonic ML is obtained, the third harmonic ML can be achieved as shown in Figure 10. At the beginning of the third harmonic, energy will be transferred among the fundamental wave, the second harmonic and the third harmonic, and their respective amplitudes will be changed alternately. Therefore, compared with the second harmonic ML, the third harmonic ML needs more cavity round-trips to reach stabilization.

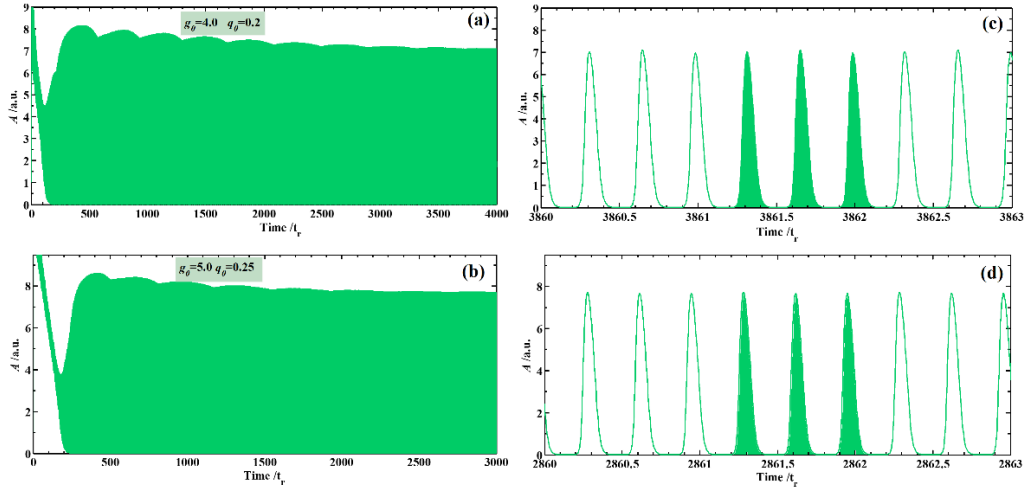

Figure 10. Third harmonic ML under different permutations of g_0 and q_0. (**a**) g_0 = 4.0, q_0 = 0.2, (**b**) g_0 = 5.0, q_0 = 0.25. (**c**,**d**) on the right side are their corresponding pulses within three round-trips.

Figure 11a–c describe the occurrence and evolution of the second and third pulse in the cavity when g_0 = 5.0 and q_0 = 0.25. (a) shows that the second pulse is split on the right side of the first pulse before about 200 intracavity cycles. (b) depicts that the third pulse is generated on the left side of the first pulse after about 200 intracavity round-trips. (c) indicates the evolution tendency of amplitudes of the first, second and third pulses. (d) shows the amplitude of three pulses circulating in cavity and the corresponding changes of absorption and gain when the third harmonic ML is stable.

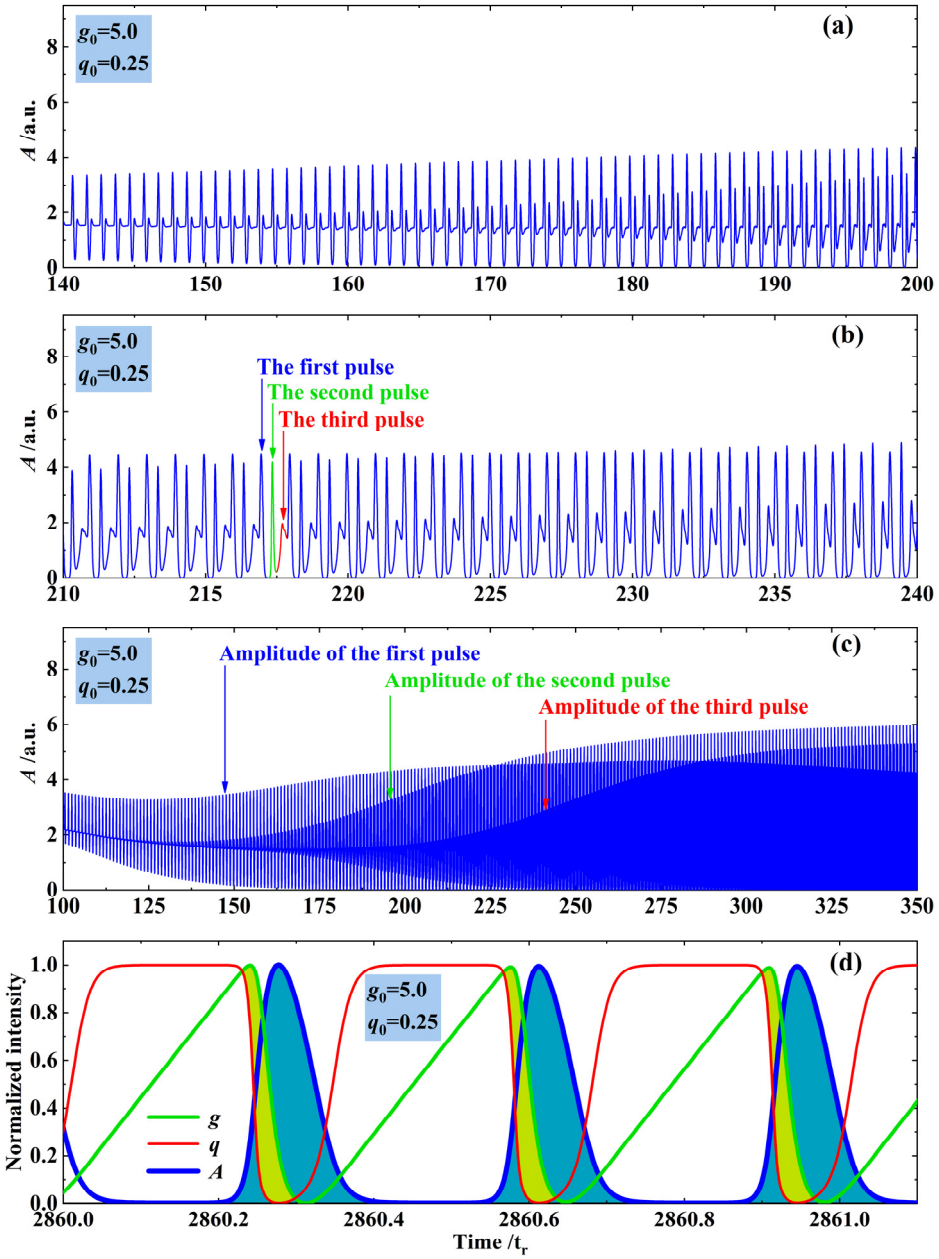

Figure 11. The occurrence and evolution of second (**a**) and third (**b**) pulse in cavity when g_0 = 5.0 and q_0 = 0.25. (**c**) The evolution tendency of amplitudes of the first, second and third pulses. (**d**) The amplitude of three pulses circulating in cavity and the corresponding changes of absorption and gain when the third harmonic ML is stable.

We summarize the second harmonic ML in Figure 8 and the third harmonic ML in Figure 10 together, plotting it in Figure 12. The x-, y- and z-axis represent g_0, q_0 and the amplitude of electric field of mode-locked pulse, and the color bar on the right side represents the pulse width. In general, with increased g_0 and q_0, the pulse width in harmonic ML decreases,

which is contrary to CW ML. The critical boundary of second and third harmonic ML is about $g_0 \cdot q_0 = 0.6$. When $g_0 \cdot q_0 < 0.6$, there are two pulses circling in the cavity, and when $g_0 \cdot q_0 > 0.6$, the third harmonic ML happens.

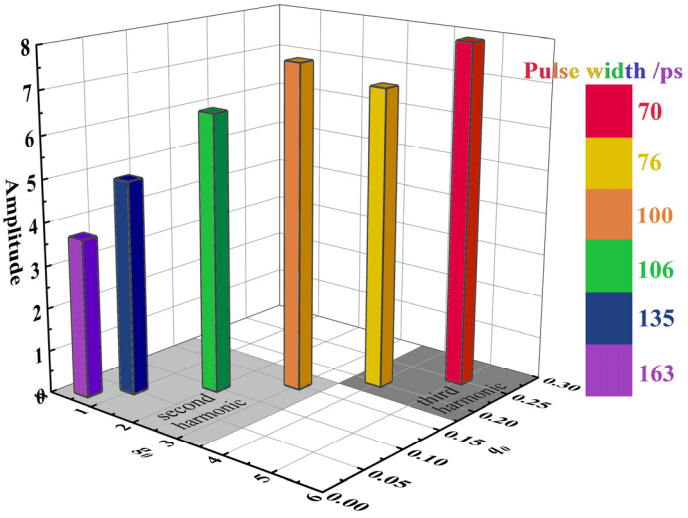

Figure 12. Second and third harmonic ML under different permutations of g_0 and q_0. The critical boundary of second and third harmonic ML is about $g_0 \cdot q_0 = 0.6$.

Harmonic ML in a self-mode-locked SDL has been realized experimentally [21]. ML was initiated by using a variable slit in front of one end mirror. In the fundamental mode-locked operation, the slit could be opened completely, while in the harmonic operation, ML was only achieved with the slit partially closed. For the harmonic ML, an increased pump power was required to achieve higher harmonics. The reported experimental results show that when the fundamental ML was achieved, larger saturable absorption and higher pump intensity, which means higher q_0 and g_0, was needed for harmonic ML, and these results are consistent with our simulations.

At last, the theoretical laser threshold (given by $g = q - \ln(\kappa)$), the calculated Q-switched ML threshold, CW ML threshold and harmonic ML threshold are generalized in Figure 13. For fixed q_0, after g_0 exceeding the laser threshold, continually increased g_0 will result the occurrence of Q-switched ML. CW ML can be obtained by further increasing g_0, and the boundary of transition is g_0~1.5–2 q_0. The region of CW ML is significantly larger than that of Q-switch ML. When g_0 goes beyond 15–20 q_0, CW ML will evolve to harmonic ML. Obviously, the range of harmonic ML is minimal.

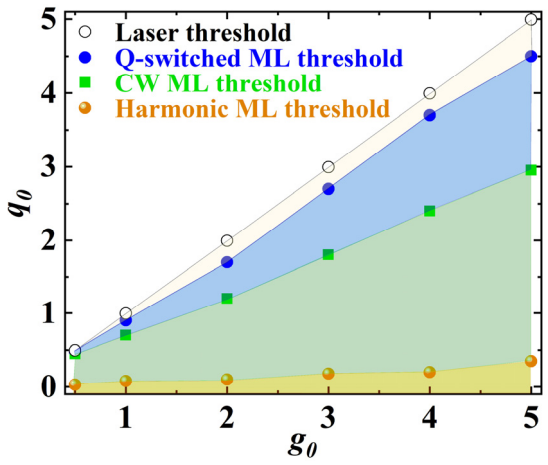

Figure 13. Theoretical laser threshold, calculated Q-switched ML threshold, CW ML threshold and harmonic ML threshold.

4. Conclusions

In conclusion, we have performed the dynamics simulation of SML in a SDL using DDEs. Occurrence conditions and evolution characteristics of Q-switched ML, CW ML and harmonic ML are calculated and numerically analyzed. It has been found that the relatively small g_0 just above laser threshold is the main reason for the undersaturated process of saturable absorption, which leads to Q-switching. CW ML can be obtained by increasing g_0 continuously, and the boundary of transition is g_0~1.5–2 q_0. When g_0 goes beyond 15–20 q_0, CW ML will evolve to harmonic ML. The critical boundary of second and third harmonic ML is about $g_0 \cdot q_0 = 0.6$. This kind of numerical simulation and analysis provides some understanding of the dynamics process of SML, and may be referenced for related experiments.

Author Contributions: Conceptualization, T.W. and P.Z.; methodology, T.W.; software, T.W. and Y.L.; validation, C.T.; formal analysis, R.Z. and T.W.; writing—original draft preparation, T.W.; writing—review and editing, P.Z.; supervision, P.Z.; project administration, P.Z.; funding acquisition, P.Z., T.W. and C.T. All authors have read and agreed to the published version of the manuscript.

Funding: This research was funded by the Cooperation Project between Chongqing Local Universities and Institutions of Chinese Academy of Sciences, Chongqing Municipal Education Commission, grant number HZ2021007; the National Natural Science Foundation of China, grant number 61904024, 61975003 and 61790584; the Science and Technology Research Program of Chongqing Municipal Education Commission, grant number KJZD-M201900502; and the State Key Laboratory of Luminescence and Applications, grant number SKLA-2019-04.

Institutional Review Board Statement: Not applicable.

Informed Consent Statement: Not applicable.

Data Availability Statement: Not applicable.

Conflicts of Interest: The authors declare no conflict of interest.

References

1. Keller, U.; Tropper, A.C. Passively mode-locked surface-emitting semiconductor lasers. *Phys. Rep.* **2006**, *429*, 67–120. [CrossRef]
2. Rahimi-Iman, A. Recent advances in VECSELs. *J. Optics-UK* **2016**, *18*, 093003. [CrossRef]
3. Guina, M.; Rantamäki, A.; Härkönen, A. Optically pumped VECSELs: Review of technology and progress. *J. Phys. D Appl. Phys.* **2017**, *50*, 383001. [CrossRef]
4. Tilma, B.W.; Mangold, M.; Zaugg, C.A.; Link, S.M.; Waldburger, D.; Klenner, A.; Mayer, A.S.; Gini, E.; Golling, M.; Keller, U. Recent advances in ultrafast semiconductor disk lasers. *Light Sci. Appl.* **2015**, *4*, e310. [CrossRef]
5. Gaafar, M.A.; Rahimi-Iman, A.; Fedorova, K.A.; Stolz, W.; Rafailov, E.U.; Koch, M. Mode-locked semiconductor disk lasers. *Adv. Opt. Photonics* **2016**, *8*, 370–400. [CrossRef]
6. Voigt, F.F.; Emaury, F.; Bethge, P.; Waldburger, D.; Link, S.M.; Carta, S.; van der Bourg, A.; Helmchen, F.; Keller, U. Multiphoton in vivo imaging with a femtosecond semiconductor disk laser. *Biomed. Opt. Express* **2017**, *8*, 3213–3231. [CrossRef] [PubMed]
7. Link, S.M.; Maas, D.J.H.C.; Waldburger, D.; Keller, U. Dual-comb spectroscopy of water vapor with a free-running semiconductor disk laser. *Science* **2017**, *356*, 1164–1168. [CrossRef]
8. Tinsley, J.N.; Bandarupally, S.; Penttinen, J.P.; Manzoor, S.; Ranta, S.; Salvi, L.; Guina, M.; Poli, N. Watt-level blue light for precision spectroscopy, laser cooling and trapping of strontium and cadmium atoms. *Opt. Express* **2021**, *29*, 25462–25476. [CrossRef]
9. Hoogland, S.; Dhanjal, S.; Tropper, A.C.; Roberts, J.S.; Haring, R.; Paschotta, R.; Morier-Genoud, F.; Keller, U. Passively mode-locked diode-pumped surface-emitting semiconductor laser. *IEEE Photonic. Tech. Lett.* **2000**, *12*, 1135–1137. [CrossRef]
10. Rudin, B.; Wittwer, V.J.; Maas, D.J.H.C.; Hoffmann, M.; Sieber, O.D.; Barbarin, Y.; Golling, M.; Südmeyer, T.; Keller, U. High-power MIXSEL: An integrated ultrafast semiconductor laser with 6.4 W average power. *Opt. Express* **2010**, *18*, 27582–27588. [CrossRef]
11. Quarterman, A.H.; Wilcox, K.G.; Apostolopoulos, V.; Mihoubi, Z.; Elsmere, S.P.; Farrer, I.; Ritchie, D.A.; Tropper, A. A passively mode-locked external-cavity semiconductor laser emitting 60-fs pulses. *Nat. Photonics* **2009**, *3*, 729–731. [CrossRef]
12. Mangold, M.; Zaugg, C.A.; Link, S.M.; Golling, M.; Tilma, B.W.; Keller, U. Pulse repetition rate scaling from 5 to 100 GHz with a high-power semiconductor disk laser. *Opt. Express* **2014**, *22*, 6099–6107. [CrossRef] [PubMed]
13. Paschotta, R.; Häring, R.; Garnache, A.; Hoogland, S.; Tropper, A.C.; Keller, U. Soliton-like pulse-shaping mechanism in passively mode-locked surface-emitting semiconductor lasers. *Appl. Phys. B* **2002**, *75*, 445–451. [CrossRef]
14. Kilen, I.; Hader, J.; Moloney, J.V.; Koch, S.W. Ultrafast nonequilibrium carrier dynamics in semiconductor laser mode locking. *Optica* **2014**, *1*, 192–197. [CrossRef]

15. Shang, X.; Xu, N.; Zhang, H.; Li, D. Nonlinear photoresponse of high damage threshold titanium disulfide nanocrystals for Q-switched pulse generation. *Opt. Laser Technol.* **2022**, *151*, 107988. [CrossRef]
16. Li, Y.; Zhang, J.; Jia, Z.; Liu, Y.; Nie, H.; Zhang, B.; Tao, X. Growth, thermal and spectroscopic properties, and continuous-wave laser performance of Tm, Ho: GGAG crystal for ~ 2 μm lasers. *J. Cryst. Growth* **2022**, *601*, 126948. [CrossRef]
17. Xu, N.; Wang, H.; Zhang, H.; Guo, L.; Shang, X.; Jiang, S.; Li, D. Palladium diselenide as a direct absorption saturable absorber for ultrafast mode-locked operations: From all anomalous dispersion to all normal dispersion. *Nanophotonics* **2020**, *9*, 4295–4306. [CrossRef]
18. Pang, L.; Sun, Z.; Zhao, Q.; Wang, R.; Yuan, L.; Wu, R.; Lv, Y.; Liu, W. Ultrafast Photonics of Ternary $Re_xNb_{(1-x)}S_2$ in Fiber Lasers. *ACS Appl. Mater. Inter.* **2021**, *13*, 28721–28728. [CrossRef]
19. Kornaszewski, L.; Maker, G.; Malcolm, G.P.; Butkus, M.; Rafailov, E.U.; Hamilton, C.J. SESAM-free mode-locked semiconductor disk laser. *Laser Photonics Rev.* **2012**, *6*, L20–L23. [CrossRef]
20. Gaafar, M.; Richter, P.; Keskin, H.; Möller, C.; Wichmann, M.; Stolz, W.; Rahimi-Iman, A.; Koch, M. Self-mode-locking semiconductor disk laser. *Opt. Express* **2014**, *22*, 28390–28399. [CrossRef]
21. Gaafar, M.; Möller, C.; Wichmann, M.; Heinen, B.; Kunert, B.; Rahimi-Iman, A.; Stolz, W.; Koch, M. Harmonic self-mode-locking of optically pumped semiconductor disc laser. *Electron. Lett.* **2014**, *50*, 542–543. [CrossRef]
22. Moloney, J.V.; Kilen, I.; Baumner, A.; Scheller, M.; Koch, S.W. Nonequilibrium and thermal effects in mode-locked VECSELS. *Opt. Express* **2014**, *22*, 6422–6427. [CrossRef] [PubMed]
23. Bek, R.; Großmann, M.; Kahle, H.; Koch, M.; Rahimi-Iman, A.; Jetter, M.; Michler, P. Self-mode-locked AlGaInP-VECSEL. *Appl. Phys. Lett.* **2017**, *111*, 182105. [CrossRef]
24. Tsou, C.H.; Liang, H.C.; Huang, K.F.; Chen, Y.F. Observation of reflection feedback induced the formation of bright-dark pulse pairs in an optically pumped semiconductor laser. *Opt. Express* **2016**, *24*, 13000–13008. [CrossRef] [PubMed]
25. Chen, Y.F.; Lee, Y.C.; Liang, H.C.; Lin, K.Y.; Su, K.W.; Huang, K.F. Femtosecond high-power spontaneous mode-locked operation in vertical-external cavity surface-emitting laser with gigahertz oscillation. *Opt. Lett.* **2011**, *36*, 4581–4583. [CrossRef]
26. Albrecht, A.R.; Wang, Y.; Ghasemkhani, M.; Seletskiy, D.V.; Cederberg, J.G.; Sheik-Bahae, M. Exploring ultrafast negative Kerr effect for mode-locking vertical external-cavity surface-emitting lasers. *Opt. Express* **2013**, *21*, 28801–28808. [CrossRef] [PubMed]
27. Kriso, C.; Kress, S.; Munshi, T.; Grossmann, M.; Bek, R.; Jetter, M.; Michler, P.; Stolz, W.; Koch, M.; Rahimi-Iman, A. Microcavity-enhanced Kerr nonlinearity in a vertical-external-cavity surface-emitting laser. *Opt. Express* **2019**, *27*, 11914–11929. [CrossRef]
28. Morgner, U.; Kärtner, F.X.; Cho, S.H.; Chen, Y.; Haus, H.A.; Fujimoto, J.G.; Ippen, E.P.; Scheuer, V.; Angelow, G.; Tschudi, T. Sub-two-cycle pulses from a Kerr-lens mode-locked Ti: Sapphire laser. *Opt. Lett.* **1999**, *24*, 411–413. [CrossRef]
29. Keller, U.; Weingarten, K.J.; Kartner, F.X.; Kopf, D.; Braun, B.; Jung, I.D.; Fluck, R.; Honninger, C.; Matuschek, N.; Der Au, J.A. Semiconductor saturable absorber mirrors (SESAM's) for femtosecond to nanosecond pulse generation in solid-state lasers. *IEEE J. Sel. Top. Quant.* **1996**, *2*, 435–453. [CrossRef]
30. Kilen, I.; Koch, S.W.; Hader, J.; Moloney, J.V. Non-equilibrium ultrashort pulse generation strategies in VECSELs. *Optica* **2017**, *4*, 412–417. [CrossRef]
31. McLaren, S.; Kilen, I.; Moloney, J.V. Microscopic modeling of transverse mode instabilities in mode-locked vertical external-cavity surface-emitting lasers. *Appl. Phys. Lett.* **2020**, *116*, 031102. [CrossRef]
32. Saarinen, E.J.; Härkönen, A.; Herda, R.; Suomalainen, S.; Orsila, L.; Hakulinen, T.; Guina, M.; Okhotnikov, O.G. Harmonically mode-locked VECSELs for multi-GHz pulse train generation. *Opt. Express* **2007**, *15*, 955–964. [CrossRef]
33. Hausen, J.; Lüdge, K.; Gurevich, S.V.; Javaloyes, J. How carrier memory enters the Haus master equation of mode-locking. *Opt. Lett.* **2020**, *45*, 6210–6213. [CrossRef] [PubMed]
34. Butkus, M.; Viktorov, E.A.; Erneux, T.; Hamilton, C.J.; Maker, G.; Malcolm, G.P.A.; Rafailov, E.U. 85.7 MHz repetition rate mode-locked semiconductor disk laser: Fundamental and soliton bound states. *Opt. Express* **2013**, *21*, 25526–25531. [CrossRef] [PubMed]
35. Hausen, J.; Meinecke, S.; Lingnau, B.; Lüdge, K. Pulse cluster dynamics in passively mode-locked semiconductor vertical-external-cavity surface-emitting lasers. *Phys. Rev. Appl.* **2019**, *11*, 044055. [CrossRef]
36. Schelte, C.; Hessel, D.; Javaloyes, J.; Gurevich, S.V. Dispersive instabilities in passively mode-locked integrated external-cavity surface-emitting lasers. *Phys. Rev. Appl.* **2020**, *13*, 054050. [CrossRef]
37. Avrutin, E.A.; Panajotov, K. Delay-differential-equation modeling of mode- locked vertical-external-cavity surface-emitting lasers in different cavity configurations. *Materials* **2019**, *12*, 3224. [CrossRef]
38. Haus, H.A. Mode-locking of lasers. *IEEE J. Sel. Top. Quant.* **2000**, *6*, 1173–1185. [CrossRef]
39. Vladimirov, A.G.; Turaev, D.; Kozyreff, G. Delay differential equations for mode-locked semiconductor lasers. *Opt. Lett.* **2004**, *29*, 1221–1223. [CrossRef] [PubMed]
40. Vladimirov, A.G.; Turaev, D. Model for passive mode locking in semiconductor lasers. *Phys. Rev. A* **2005**, *72*, 033808. [CrossRef]
41. Arkhipov, R.; Pimenov, A.; Radziunas, M.; Rachinskii, D.; Vladimirov, A.G.; Arsenijević, D.; Schmeckebier, H.; Bimberg, D. Hybrid mode locking in semiconductor lasers: Simulations, analysis, and experiments. *IEEE J. Sel. Top. Quant.* **2012**, *19*, 1100208. [CrossRef]
42. Quarterman, A.H.; Tyrk, M.A.; Wilcox, K.G. Z-scan measurements of the nonlinear refractive index of a pumped semiconductor disk laser gain medium. *Appl. Phys. Lett.* **2015**, *106*, 011105. [CrossRef]

43. Huang, D.; Ulman, M.; Acioli, L.H.; Haus, H.A.; Fujimoto, J.G. Self-focusing-induced saturable loss for laser mode locking. *Opt. Lett.* **1992**, *17*, 511–513. [CrossRef] [PubMed]
44. Brabec, T.; Spielmann, C.; Curley, P.F.; Krausz, F. Kerr lens mode locking. *Opt. Lett.* **1992**, *17*, 1292–1294. [CrossRef] [PubMed]
45. Kriso, C.; Bergmeier, T.; Giannini, N.; Albrecht, A.R.; Sheik-Bahae, M.; Benis, S.; Faryadras, S.; van Stryland, E.W.; Hagan, D.J.; Koch, M.; et al. Probing the ultrafast gain and refractive index dynamics of a VECSEL. *Appl. Phys. Lett.* **2021**, *119*, 191105. [CrossRef]